THE JOURNAL OF BIOLOGICAL CHEMISTRY VOL. 286, NO. 1, pp. 707–716, January 7, 2011

KCNQ1 Channels Voltage Dependence through a Voltage-dependent Binding of the S4-S5 Linker to the Pore Domain*[S]

Received for publication, May 19, 2010, and in revised form, October 1, 2010 Published, JBC Papers in Press, October 12, 2010, DOI 10.1074/jbc.M110.146324

Frank S. Choveau[‡§¶1], Nicolas Rodriguez[‡§¶], Fayal Abderemane Ali[‡§¶], Alain J. Labro[‖], Thierry Rose[**], Shehrazade Dahimène[‡§¶2], Hélène Boudin[¶‡‡§§3], Carole Le Hénaff[‡§¶4], Denis Escande[†‡§¶], Dirk J. Snyders[‖], Flavien Charpentier[‡§¶3], Jean Mérot[‡§¶5], Isabelle Baró[‡§¶5], and Gildas Loussouarn[‡§¶5,6]

From [‡]INSERM, U915, Nantes F-44000, France, [§]CNRS, ERL3147, Nantes F-44035, France, [¶]Université de Nantes, Faculté de Médecine, l'Institut du Thorax, Nantes F-44000, France, the [‖]Department of Biomedical Sciences, Laboratory for Molecular Biophysics, Physiology, and Pharmacology, University of Antwerp, 2610 Antwerp, Belgium, [**]Institut Pasteur, Plate-forme de Biophysique des Macromolécules et de leurs Interactions, 25 rue du Dr. Roux, 75724 Paris Cedex 15, France, [‡‡]INSERM, U643, Nantes F-44000 France, and [§§]CHU Nantes, Institut de Transplantation et de Recherche en Transplantation, Nantes F-44000, France

Voltage-dependent potassium (Kv) channels are tetramers of six transmembrane domain (S1–S6) proteins. Crystallographic data demonstrate that the tetrameric pore (S5–S6) is surrounded by four voltage sensor domains (S1–S4). One key question remains: how do voltage sensors (S4) regulate pore gating? Previous mutagenesis data obtained on the Kv channel KCNQ1 highlighted the critical role of specific residues in both the S4-S5 linker ($S4S5_L$) and S6 C terminus ($S6_T$). From these data, we hypothesized that $S4S5_L$ behaves like a ligand specifically interacting with $S6_T$ and stabilizing the closed state. To test this hypothesis, we designed plasmid-encoded peptides corresponding to portions of $S4S5_L$ and $S6_T$ of the voltage-gated potassium channel KCNQ1 and evaluated their effects on the channel activity in the presence and absence of the ancillary subunit KCNE1. We showed that $S4S5_L$ peptides inhibit KCNQ1, in a reversible and state-dependent manner. $S4S5_L$ peptides also inhibited a voltage-independent KCNQ1 mutant. This inhibition was competitively prevented by a peptide mimicking $S6_T$, consistent with $S4S5_L$ binding to $S6_T$. Val^{254} in $S4S5_L$ is known to contact Leu^{353} in $S6_T$ when the channel is closed, and mutations of these residues alter the coupling between the two regions. The same mutations introduced in peptides altered their effects, further confirming $S4S5_L$ binding to $S6_T$. Our results suggest a mechanistic model in which $S4S5_L$ acts as a voltage-dependent ligand bound to its receptor on S6 at rest. This interaction locks the channel in a closed state. Upon plasma membrane depolarization, S4 pulls $S4S5_L$ away from $S6_T$, allowing channel opening.

Voltage-gated ion channels are ubiquitously expressed in human tissues where they play diverse physiological functions such as generation and modulation of the electrical activity in excitable tissues, myocyte contraction, modulation of neurotransmitter and hormone release, and electrolyte transport in epithelia. Crystallization and x-ray diffraction of both a prokaryote and a mammalian voltage-gated potassium (Kv) channel provided a lot of information on the structure of Kv channels (1–3). Even though these data initiated controversies on the dynamics of the voltage sensor, S4 (4), they provided a new template for investigations on Kv channel molecular characteristics. For example, the structure of the Kv pore domain (S5–S6) turned out to be similar to the pore domain of two-transmembrane domain potassium channels like KcsA (5) and KirBac1.1 (6). Besides structure, the crystallographic analyses of KvAP and Kv1.2 gave insights on the dynamics of channel voltage dependence. Notably, the crystal structure of Kv1.2 is believed to represent the channel in an open state (3), and in this conformation, the S4-S5 linker ($S4S5_L$)[7] is interacting with the S6 C terminus ($S6_T$). The authors (3) used homology modeling to infer a closed state structure from the open state structure. In the closed state, the model shows that $S4S5_L$ and $S6_T$ are also in contact. Those results pointed to a mechanism by which $S4S5_L$ are permanently linked to S6, and this link is critical in translating the voltage sensor movement into gate opening or closure (3).

In a few other channels, the $S4S5_L/S6_T$ interaction seems rather state-dependent. A second-site suppressor yeast screen in the hyperpolarization-activated channel KAT1 suggested that $S4S5_L$ and $S6_T$ are interacting only in the channel open state (7). In another hyperpolarization-activated channel,

* This work was supported in part by grants from the Institut National de la Santé et de la Recherche Médicale (INSERM), from the Agence Nationale de la Recherche (ANR-05-JCJC-0160-01), the Hubert Curien Program (Tournesol program), and the Association Française contre les Myopathies (Grant 14120 to G. L.), and from Vaincre La Mucoviscidose (to J. M.).

† This work was the last we discussed with D. Escande, our irreplaceable mentor (deceased November 13, 2006). Denis, thanks for your leading enthusiasm in every project.

[S] The on-line version of this article (available at http://www.jbc.org) contains supplemental Fig. 1.

[1] Supported by the Fondation Génavie, the Fondation pour la Recherche Médicale, and the Fédération Française de Cardiologie.
[2] Recipient of a grant from the French Ministère de la Recherche.
[3] Recipient of a tenure position supported by INSERM.
[4] Present address: Institut des Vaisseaux et du Sang, Hôpital Lariboisière, 8 rue Guy Patin, 75475 Paris Cedex 10, France.
[5] Recipient of a tenure position supported by CNRS.

[6] To whom correspondence should be addressed: INSERM U915, 8 quai Moncousu, BP 70721, 44007 Nantes Cedex, France. Fax: 33-2-28-08-01-30; E-mail: gildas.loussouarn@inserm.fr.

[7] The abbreviations used are: $S4S5_L$, S4-S5 linker; $S6_T$, S6 C terminus; hERG, human ether-a-go-go-related gene; HCN, hyperpolarization-activated cyclic nucleotide-gated channel.

cross-linking of $S4S5_L$ and $S6_T$ prevented the channel from deactivating (8), suggesting that $S4S5_L$ and $S6_T$ are interacting only when the channel is open. In hERG too, a cross-linking study suggested a state-dependent $S4S5_L$ and $S6_T$ interaction but, this time, in the closed state (9). In the cited studies, the state-dependent interaction between $S4S5_L$ and $S6_T$ suggests that this interaction may stabilize the open state of hyperpolarization-activated channels (KAT1, HCN) and the closed state of depolarization-activated channels (hERG).

Scanning mutagenesis studies were performed in a cardiac voltage-gated potassium channel, KCNQ1 (10, 11) to study the role of $S4S5_L$ (see companion article (31)) and $S6_T$ (12) in the voltage modulation of this channel. These studies identified residues implicated in the $S4S5_L/S6_T$ interaction. In particular, the V254A mutation in $S4S5_L$ and L353A mutation in $S6_T$ led to a similar phenotype, *i.e.* the appearance of a voltage-independent current component, suggesting that mutation of one of these residues decreases the interaction between $S4S5_L$ and $S6_T$ in the closed state. Thus, as in hERG, specific interaction between $S4S5_L$ and $S6_T$ residues may also stabilize KCNQ1 channel closed state. This would suggest that $S4S5_L$ acts as a ligand, stabilizing the channel closed state, such as ATP stabilizes the K_{ATP} channel closed state (13). To test whether $S4S5_L$ by itself is a ligand and $S6_T$ is its receptor, we have designed plasmids coding for the potential ligand ($S4S5_L$, 16 amino acids) and receptor ($S6_T$, 13 amino acids) and tested their effects on KCNQ1 function. Our results suggest that $S4S5_L$ stabilizes the channel in a closed conformation by interacting with $S6_T$. Upon depolarization of the plasma membrane, S4 pulls $S4S5_L$ away from $S6_T$, allowing channel opening.

EXPERIMENTAL PROCEDURES

Plasmid Constructs—Complementary DNAs encoding KCNQ1 peptides were amplified by polymerase chain reaction using specific primers corresponding to KCNQ1 $S4S5_L$ or $S6_T$. The PCR products were cloned into pCRII-TOPO, sequenced, and then cloned into pIRES2-EGFP (Clontech). The 5′-end of the forward primers contained a Kozak consensus sequence followed by an initiation codon (ATG) and a glycine (GGA) to protect the ribosome binding site (14). To construct the pCB6-L353A hKCNQ1, a Not1-BamH1 fragment containing the mutation was cut out of the pIRES2-EGFP-L353A hKCNQ1 (12) and ligated into pCB6-hKCNQ1 to replace the WT sequence. Sequencing of the plasmid confirmed the presence of the mutation and the absence of unwanted mutations.

Cell Culture and Transfection—The African green monkey kidney-derived cell line COS-7 was obtained from the American Type Culture Collection (CRL-1651) and cultured in Dulbecco's modified Eagle's medium (Invitrogen) supplemented with 10% fetal calf serum and antibiotics (100 international units/ml penicillin and 100 μg/ml streptomycin) at 5% CO_2 and 95% air at 37 °C in a humidified incubator. Cells were transfected in 35-mm plates when the culture reached 60–80% confluence, with DNA (2–5 μg total DNA as described below) complexed with FuGENE 6 (Roche Molecular Biochemical) according to the standard protocol recommended by the manufacturer. In most of our experiments, the peptide effects were studied on a fusion protein of the human KCNE1 linked to the N terminus of the human KCNQ1 (a kind gift of Dr Robert S. Kass, Department of Pharmacology, College of Physicians and Surgeons, Columbia University, New York, NY). In the present study, this pCDNA3.1-KCNE1-KCNQ1 construct is named the KCNE1-KCNQ1 concatemer (E1-Q1). GFP allowed the detection of cells expressing the peptide. For experiments with WT E1-Q1 or S140G E1-Q1 (WT KCNE1 fused to S140G KCNQ1), pIRES-GFP plasmids encoding $S4S5_L$, $S6_T$, or pEGFP plasmids for control cells (1.8 μg per plate) were cotransfected with the human pCDNA3.1-KCNE1-KCNQ1 (0.2 μg per plate) concatemer. In pIRES-GFP plasmids, the second cassette (GFP) is less expressed than the first cassette, guaranteeing high levels of peptides expression in fluorescent cells. For experiments with WT or L353A KCNQ1, the pIRES-GFP plasmids (4 μg per plate) were cotransfected with the human pCB6-KCNQ1 (1 μg per plate). In experiments in which two peptides were simultaneously expressed (see Fig. 7), DNA composition was 0.2 μg of pCDNA3.1-S140G E1-Q1, 0.9 μg pIRES-GFP plasmids encoding $S4S5_L$, and 0.9 μg of pIRES-GFP plasmids encoding $S6_T$ (or pCB6-CD4 (15) for control cells). In hERG experiments, COS-7 cells were co-transfected with 0.4 μg of pSI hERG (16) and 1.6 μg of pEGFP (control) or pIRES-GFP plasmids encoding a peptide ($S4S5_L$ or $S6_T$).

Electrophysiology—24 to 72 h after transfection, COS-7 cells were mounted on the stage of an inverted microscope and constantly perfused at a rate of 2 ml/min. The bath temperature was maintained at 24.0 ± 1.0 °C. Stimulation, data recording and analysis were performed by Acquis1 (Bio-Logic Science Instruments) through an analog-to-digital converter (Tecmar TM100 Labmaster; Scientific Solution). Electrodes were connected to a patch-clamp amplifier (RK-400; Bio-Logic Science Instruments). Currents were recorded in the whole-cell configuration. KCNQ1 and hERG activation curves were obtained from the tail currents and fitted by Boltzmann equations. KCNE1-KCNQ1 activation and deactivation kinetics were obtained by a monoexponential fit. If channels are spending more time in deeper closed states, they need to go through more states before reaching the open state. This is reflected by a prolonged delay in channel activation (17). This delay in channel activation was calculated from the shift in the monoexponential fit of the current measured at +80 mV.

Solutions—In ruptured patch experiments, pipettes (Kimble; Vineland, NJ) were filled with the following solution: 150 mM KCl, 10 mM HEPES, 5 mM EGTA and 0.5 mM $MgCl_2$, pH 7.2, with KOH. In permeabilized patch experiments, the pipette solution contained the following: 120 mM K-gluconate, 25 mM KCl, 10 mM HEPES, 1 mM EGTA, 0.8 μg/ml amphotericin B, pH 7.2, with KOH. The standard Tyrode perfusion solution contained the following: 145 mM NaCl, 4 mM KCl, 1 mM $CaCl_2$, 1 mM $MgCl_2$, 5 mM HEPES and 5 mM glucose, pH 7.4, with NaOH.

Kinetic Model—The KCNE1-KCNQ1 kinetic model was derived from the model described by Silva and Rudy (18). This model has been optimized using Model Maker (version 4.0, AP Benson) to fit our experimental data, with an additional constraint: P_o is <0.65 at potentials where the channel is fully activated. This constraint comes from the observation

that S6 peptide Ile^{346}–Lys^{358} can increase the maximal current by 50% (see Fig. 2). Consistent with the hypothetical mechanism, endogenous S4S5$_L$ linkers are pulled away from the binding site in the closed state preceding channel opening (Fig. 8, *A*, *panel a*). Two other models can be then designed (Fig. 8, *A*, *panels b* and *c*), with either S4S5$_L$ or S6$_T$ peptide binding to this closed state. The three models (control, S4S5$_L$, S6$_T$) were simultaneously optimized for current density, half-activation potential, activation, and deactivation kinetics using Mathematica (Wolfram Research). Optimized transition rates are presented in Table 1.

TABLE 1
Optimized transition rates used in the model presented in Fig. 8
Values are as follows: $F = 96{,}485$ C · mol^{-1} (Faraday constant); $R = 8.314$ J · mol^{-1} · K^{-1} (Gas constant); $T = 297$ K; and V (membrane potential).

Transition description	Rudy's model notation(18)	Transition rate (ms^{-1})
Voltage sensor transition rates		
Closed Locked 2 (CL2) → Closed Locked 1 (CL1)	α	$6.31 \cdot 10^{-5}$
CL1→ CL2	β	$2.182 \cdot 10^{-5} \cdot \exp\left(-0.81 \cdot 10^{-3} \cdot \frac{V \cdot F}{R \cdot T}\right)$
CL1 → Closed unlock (CU)	γ	$3.94 \cdot 10^{-3} \cdot \exp\left(0.354 \cdot \frac{V \cdot F}{R \cdot T}\right)$
CU → CL1	δ	$1.487 \cdot 10^{-3} \cdot \exp\left(-0.122 \cdot \frac{V \cdot F}{R \cdot T}\right)$
Peptide binding/unbinding transition rates		
CU → Closed locked pept. S4S5$_L$ (CLP4)		$2.881 \cdot 10^{-5}$
CLP4 → CU		$4.038 \cdot 10^{-5}$
CU → Closed unlock pept. S6$_T$ (CUP6)		$2.798 \cdot 10^{-2}$
CUP6 → CU		$9.502 \cdot 10^{-3}$
Concerted opening transition rates		
4 monomers CU or CUP6 → Open state 1 (O1)	θ	$2.985 \cdot 10^{-3}$
O1 → 4 monomers CU or CUP6	η	$8.902 \cdot 10^{-2} \cdot \exp\left(-1.072 \cdot \frac{V \cdot F}{R \cdot T}\right)$
O1 → Open state 2 (O2)	ψ	$2.084 \cdot 10^{-2} \cdot \exp\left(7.56 \cdot 10^{-2} \cdot \frac{V \cdot F}{R \cdot T}\right)$
O2 → O1	ω	$1.587 \cdot 10^{-3} \cdot \exp\left(0.392 \cdot \frac{V \cdot F}{R \cdot T}\right)$

Statistics—All data are expressed as means ± S.E. Statistical differences between samples were determined using Student's *t* tests, rank sum tests (when data were not normally distributed), and two-way analysis of variance associated with a Tukey test when needed (SigmaStat, version 2.03, SPSS, Inc.). A value of $p < 0.05$ was considered significant.

RESULTS

S4S5$_L$ Linker Peptides Inhibit KCNE1-KCNQ1 Channels—S4S5$_L$ and S6$_T$ plasmids were designed based on sequence alignment with *Shaker* (Fig. 1), in which interacting areas in the S4S5$_L$ and the S6$_T$ were suggested (19, 20). For each region, three different plasmids were designed, with the same length but different starting positions, to compensate for the inaccuracy of the alignment due to the poor similarity between KCNQ1 and *Shaker* sequences. *Black arrows* in Fig. 1 show the high impact residues studied in KCNQ1, and *red arrows* show the interacting residues Val-254 and Leu-353 (12 and see accompanying article (31)). At least one of these residues is lacking in Val^{254}–Gly^{269} and Phe^{340}–Ala^{352}. For that reason, one can suppose that these peptides will be the least efficient. To study the effect of peptides on channel activity, cDNA coding for a peptide was cotransfected with the KCNE1-KCNQ1 fusion protein cDNA (21). This fusion protein limits variability in the current characteristics caused by variable KCNQ1/KCNE1 expression ratio (22).

If the endogenous S4S5$_L$ peptide is acting like a ligand modulating channel gating, then the exogenous S4S5$_L$ peptide should also modulate the channel activity. We examined the peptide effects using the whole-cell configuration of the patch clamp technique, right after patch rupture. We show that two of the three S4S5$_L$ peptides (Trp^{248}–Ile^{263} and Leu^{251}–Leu^{266}) significantly reduced the WT KCNE1-KCNQ1 current (Fig. 2, *A* and *C*). Moreover, activation was slowed by both peptides (Fig. 2*E*), but deactivation was unaffected (Fig. 2*F*). The absence of effect of peptide Val^{254}–Gly^{269} is consistent with the fact that this peptide is missing Leu^{251}. This residue seems to play a major role in the channel voltage modulation, as its

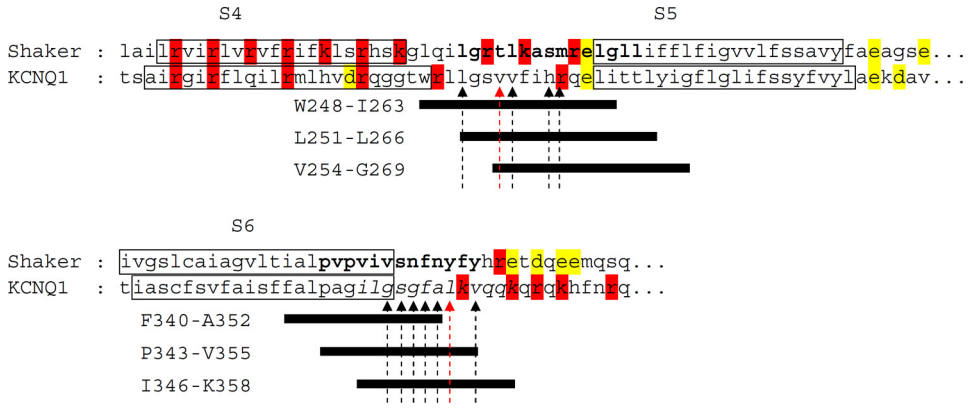

FIGURE 1. **Determination of the hypothetical voltage-dependent ligand and its binding site.** Shown is an alignment with the Shaker sequence. *Boldface letters*, interacting area in the S4S5$_L$ and the S6 C-terminal parts as suggested by Lu *et al.* (19, 20). *Black bars* represent the peptides selected to probe the ligand/binding site hypothesis. Positively and negatively charged residues are presented in *red* and *yellow*, respectively. *Arrows* show the high impact mutations (Ref. 12 and see companion article (31)).

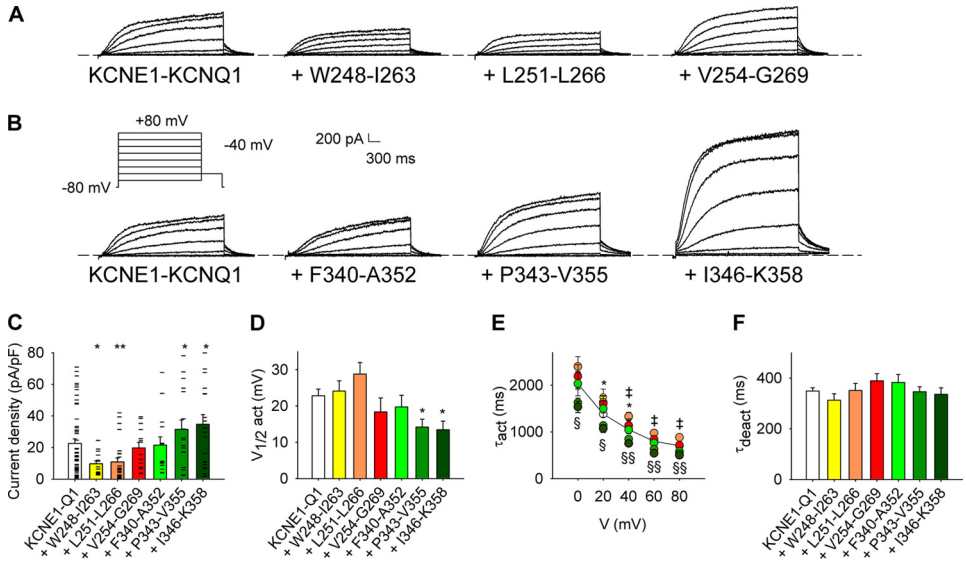

FIGURE 2. **Effects of the "S4S5$_L$ linker" or the "S6 C terminus" peptides on KCNE1-KCNQ1 currents.** *A* and *B*, representative whole-cell recordings of the WT KCNE1-KCNQ1 current in the absence (KCNE1-KCNQ1) and in the presence of S4S5$_L$ (*A*) or S6$_T$ peptides (*B*). *Inset*, voltage protocol used in *A* and *B*, one epoch every 7 s. *C–F*, average KCNE1-KCNQ1 tail current density at −40 mV after a prepulse at +80 mV (*C*), half-activation potential ($V_{1/2act}$, *D*), activation time constant at potential from 0 to +80 mV (τ_{act}, *E*), and deactivation time constant at −40 mV (τ_{deact}, *F*) in the absence and in the presence of various S4S5$_L$ or S6$_T$ peptides (n = 15–58). In *C*, current amplitude scatter data is also presented (−). *, Trp^{248}–Ile^{263}; ‡, Leu^{251}–Leu^{266}; §, Pro^{343}–Val^{355}; ¶, Ile^{346}–Lys^{358}. *One symbol*, $p < 0.05$; *two symbols*, $p < 0.01$. *Error bars* show the S.E.

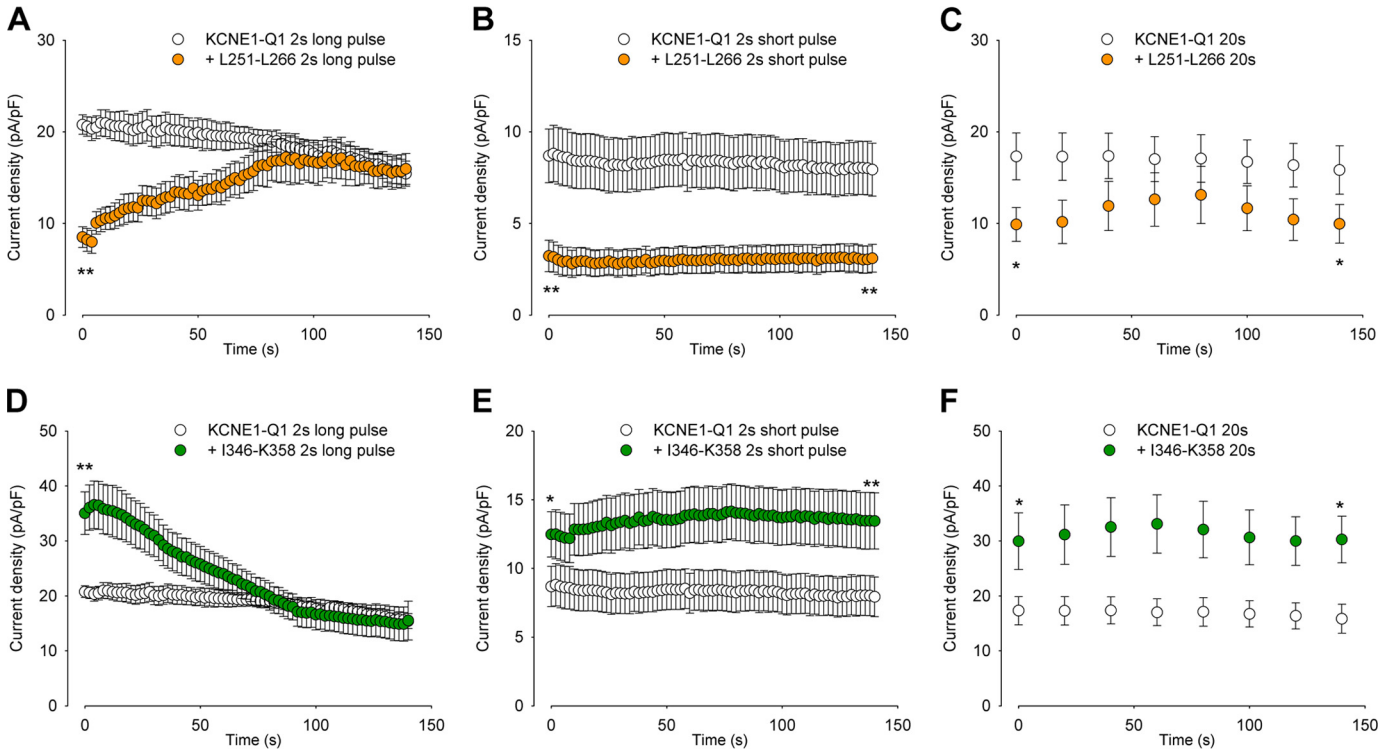

FIGURE 3. **Reversibility of the peptides effects.** *A–C*, average KCNE1-KCNQ1 tail-current density measured at −40 mV after a 250-ms to 1-s prepulse at +80 mV, as a function of time after patch rupture, in cells expressing no peptide (KCNE1-KCNQ1) or the Leu^{251}–Leu^{266} peptide. Both voltage pulse duration (*A*, 1 s; *B*, 250 ms) and depolarization frequencies were varied (*A*, a depolarization every 2 s; *C*, a depolarization every 20 s). Resting potential was −80 mV (n = 8–38). *D–F*, same experiments as in *A–C*, with the Ile^{346}–Lys^{358} peptide (n = 8–28). *, $p < 0.05$; **, $p < 0.01$ *versus* KCNE1-KCNQ1 alone.

mutation to an alanine has a high impact on the channel voltage dependence (*cf.* Fig. 1 and see companion article (31)).

S6 C Terminus Peptides Activate KCNE1-KCNQ1 Channels—If the S6 C terminus is the receptor for S4S5$_L$, then the S6$_T$ peptides should decoy the endogenous S4S5$_L$ linker, prevent its binding to S6$_T$, and increase channel activity. Indeed, two of them (Pro^{343}–Val^{355} and Ile^{346}–Lys^{358}) up-regulated the WT channel and shifted the half-activation potential toward negative values (Fig. 2, *B–D*). Activation was accelerated (Fig. 2*E*), but deactivation was unaffected (Fig. 2*F*). The absence of effect of peptide Phe^{340}–Ala^{352} is consistent with the fact that this peptide is missing Leu^{353} and Val^{355}. These residues seem

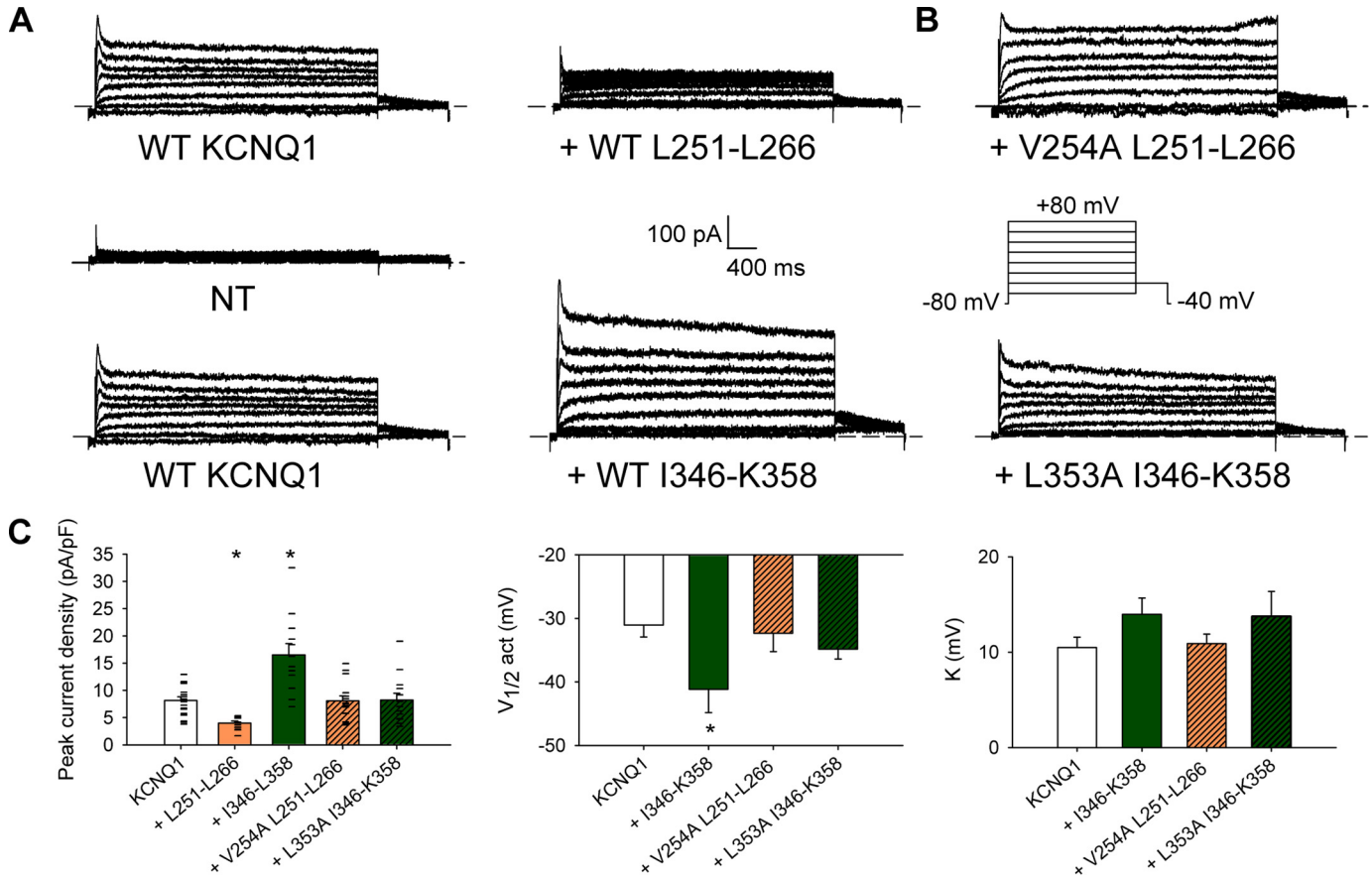

FIGURE 4. **Effects of WT and mutant $S4S5_L$ or $S6_T$ peptides on KCNQ1 currents.** *A*, representative whole-cell recordings of nontransfected cells (*NT*) and WT KCNQ1 current in the absence (KCNQ1) and in the presence of the $S4S5_L$ peptide (+ Leu^{251}–Leu^{266}) or the $S6_T$ peptide (+ Ile^{346}–Lys^{358}). *Inset*, voltage protocol, one epoch every 7 s. *B*, representative whole-cell recordings of the WT KCNQ1 current in the presence of a mutant $S4S5_L$ peptide (+ V254A Leu^{251}–Leu^{266}) or a mutant S6 C terminus peptide (+ L353A Ile^{346}–Lys^{358}). *C*, average KCNQ1 peak current density at +80 mV, half-activation potential ($V_{1/2}$) and slope (*K*) in the conditions shown in A and B ($n = 5$ for nontransfected cells, 10–18 otherwise). In *C*, current amplitude scatter data are also presented (−). *, $p < 0.05$ *versus* KCNQ1 alone.

to play a major role in the channel voltage modulation because their substitutions to an alanine have a high impact on channel voltage dependence (*cf.* Fig. 1 and Ref. 12).

Use- and State-dependent Reversibility of Peptide Effects—In the following experiments, we studied the most potent inhibiting peptide Leu^{251}–Leu^{266} and the most potent activating peptide Ile^{346}–Lys^{358} in greater details. We first analyzed the reversibility of the effects, as peptides were diffusing out of the cytosol and into the pipette after patch rupture (Fig. 3, *A* and *D*). In cells expressing KCNE1-KCNQ1 alone, the current was quite stable with a slight rundown (23). In cells coexpressing the channel and the Leu^{251}–Leu^{266} peptide, the current density increased to reach control values measured in absence of peptide (Fig. 3*A*). Conversely, in cells coexpressing the channel and the Ile^{346}–Lys^{358} peptide, the current density decreased to reach control values (Fig. 3*D*). This suggests that both peptides do not act on channel trafficking but strictly on gating.

Because any bound peptide ($S4S5_L$ or $S6_T$) is most probably intercalated between the endogenous $S4S5_L$ and $S6_T$ (*cf.* scheme in Fig. 8*A*), membrane depolarization, which pulls on the endogenous $S4S5_L$, may free the peptide that is otherwise trapped in the core of the protein. In other words, long and frequent depolarization should favor reversion; shorter or less frequent depolarization should have less effect. To test this, a shorter depolarizing pulse was applied with maintained frequency. In this condition, no reversion was observed for both the inhibiting peptide Leu^{251}–Leu^{266} (Fig. 3*C*) and the activating peptide Ile^{346}–Lys^{358} (Fig. 3*E*). We also tested a depolarizing pulse with maintained duration but lower frequency. Again, no reversion was observed (Fig. 3, *D* and *F*). Altogether, these results suggest that peptide unbinding is favored by membrane depolarization, consistent with the state-dependent channel/peptide interaction.

Effect of Peptides on KCNQ1 without KCNE1—Several studies suggest that KCNE1 interacts with $S4S5_L$ (24) and $S6_T$ (24, 25). To evaluate the role of KCNE1 in the ligand/receptor mechanism, we coexpressed the most potent peptides (Leu^{251}–Leu^{266} for $S4S5_L$ and Ile^{346}–Lys^{358} for $S6_T$) with KCNQ1 alone. Like in the presence of KCNE1, we observed a current inhibition with Leu^{251}–Leu^{266} and an activating effect with Ile^{346}–Lys^{358} (Fig. 4, *A* and *C*). These results suggest that the $S4S5_L/S6_T$ state-dependent interaction is independent of the presence/absence of KCNE1.

Mutations That Decrease $S4S5_L$ and $S6_T$ Interaction also Alter Peptide Effect—Altogether, the data presented above support the hypothesis that $S4S5_L$ peptides target the channel $S6_T$ and vice versa. To further address the specificity of the

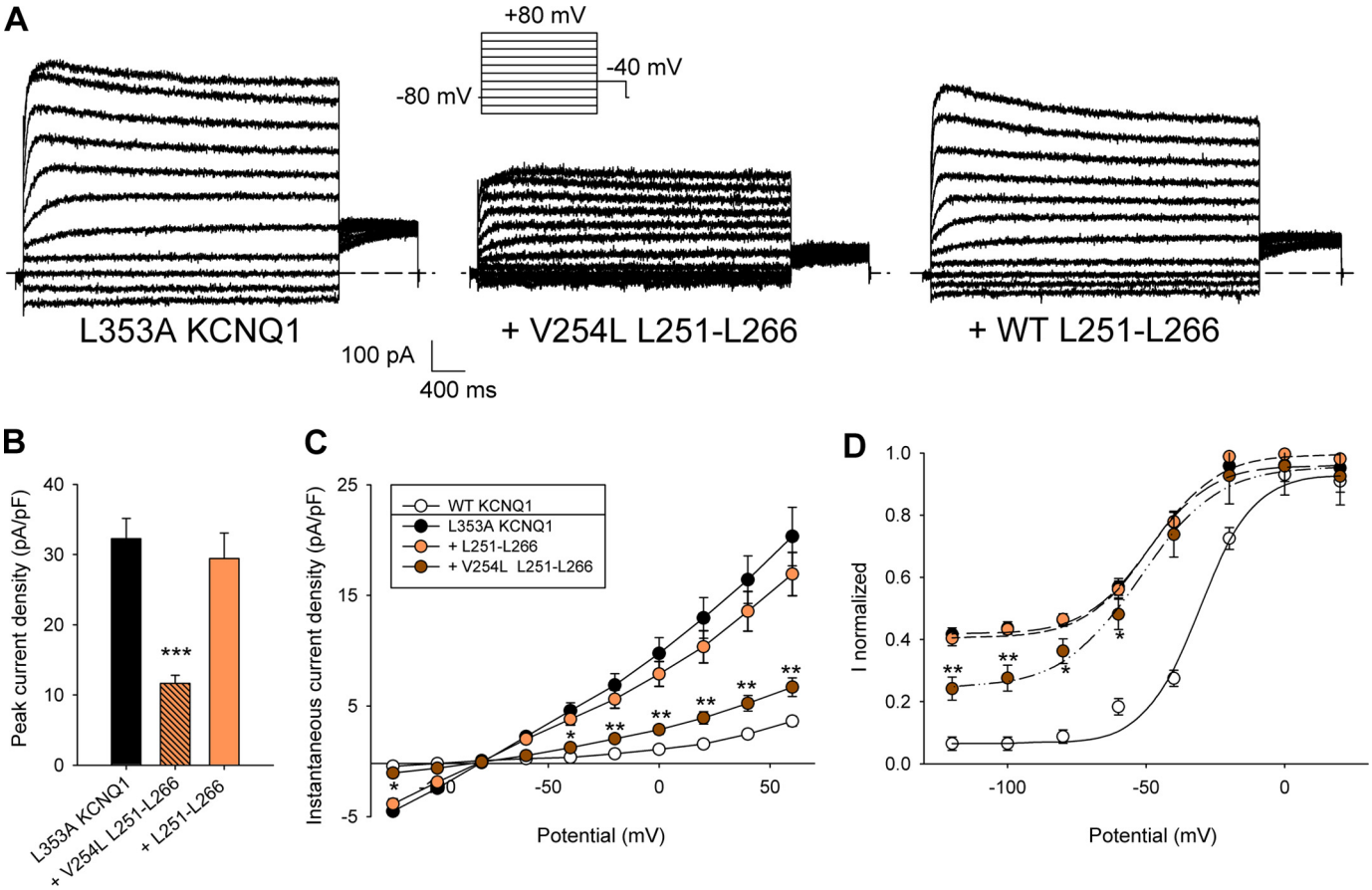

FIGURE 5. **Effects of WT and mutant S4S5$_L$ peptides on L353A KCNQ1 currents.** *A*, representative whole-cell recordings of L353A KCNQ1 current in the absence (KCNQ1 L353A) and in the presence of the mutant (+ Leu^{251}–Leu^{266} V254L) or the WT S4S5$_L$ peptide (+ Leu^{251}–Leu^{266}). *Inset*, voltage protocol, one epoch every 7 s. *B*, mean peak current density, in the three conditions described in *A* (n = 10–12). *C*, instantaneous current density, measured at the beginning of the prepulse, as a function of prepulse potential (n = 10–12). *D*, activation curve built from the tail currents at −40 mV (n = 10–12). In *C* and *D*, besides the three conditions described in *A*, KCNQ1 data are shown for comparison. *, $p < 0.05$; **, $p < 0.01$; ***, $p < 0.001$ *versus* L353A KCNQ1 alone.

interaction between the peptides and the channel, we evaluated the effect of peptides bearing mutations known to decrease S4S5$_L$ and S6$_T$ interaction. In an accompanying paper, Snyders and co-workers (31) show that the V254A mutation in S4S5$_L$ and the L353A mutation in S6$_T$ generate an instantaneous current component, suggesting that S4S5$_L$/S6$_T$ interaction is weakened by the mutations (see companion article (31)). Indeed, introduction of the V254A mutation into the S4S5$_L$ peptide Leu^{251}–Leu^{266} abolished the peptide inhibition of the channel. Similarly, introduction of the L353A mutation into the S6$_T$ peptide Ile^{346}–Lys^{358} abolished its activating effect. The suppression of both peptide effects (Fig. 4, *B* and *C*) supports that the S4S5$_L$ peptide is specifically targeting S6$_T$, and vice versa. Looking now at the channel, introduction of the L353A mutation should also render the channel less sensitive to the WT S4S5$_L$ peptide. Indeed, the peak current measured in the mutant channel L353A was not decreased when the WT S4S5$_L$ peptide was coexpressed (Fig. 5, *A* and *B*), also suggesting that the S4S5$_L$ peptide is specifically targeting S6$_T$.

Rescue of L353A Channel Closure by V254L Peptide Further Supports Peptide Specificity—In the companion article (31), the partial open phenotype of the L353A mutant channel could be rescued by the V254L mutation in the channel S4S5$_L$. In parallel, in the experiments with peptides, introduction of the V254L mutation in the S4S5$_L$ peptide restored its effect on the L353A mutant channel (Fig. 5, *A* and *B*). Moreover, the instantaneous current observed in L353A (*cf.* companion article (31)) was also reduced by the V254L S4S5$_L$ peptide but not by the WT S4S5$_L$ peptide (Fig. 5*C*). This reduction of the instantaneous current could also be observed in the activation curve (Fig. 5*D*). These experiments strictly mimicked the rescue of the S4S5$_L$/S6$_T$ interaction observed within the channel by Labro *et al.* (see companion article (31)) and is a strong support for a specific interaction between the channel and the peptide.

S4S5$_L$ Peptide Effect on a Voltage-independent Mutant—The S140G E1-Q1 mutant (WT KCNE1 fused to S140G KCNQ1) does not show any voltage dependence in the −80 to +80 mV range (26). If S4S5$_L$ peptides bind to S6$_T$ to stabilize the closed state, they should inhibit the mutant channel as well. Fig. 6 shows that coexpression of the S140G E1-Q1 mutant channel with the S4S5$_L$ peptides (Trp^{248}–Ile^{263} or Leu^{251}–Leu^{266}) led to an almost complete inhibition of the current (Fig. 6, *A* and *B*), whereas the activating peptides had no effect on the already fully activated S140G channel. In cells expressing the inhibitory S4S5$_L$

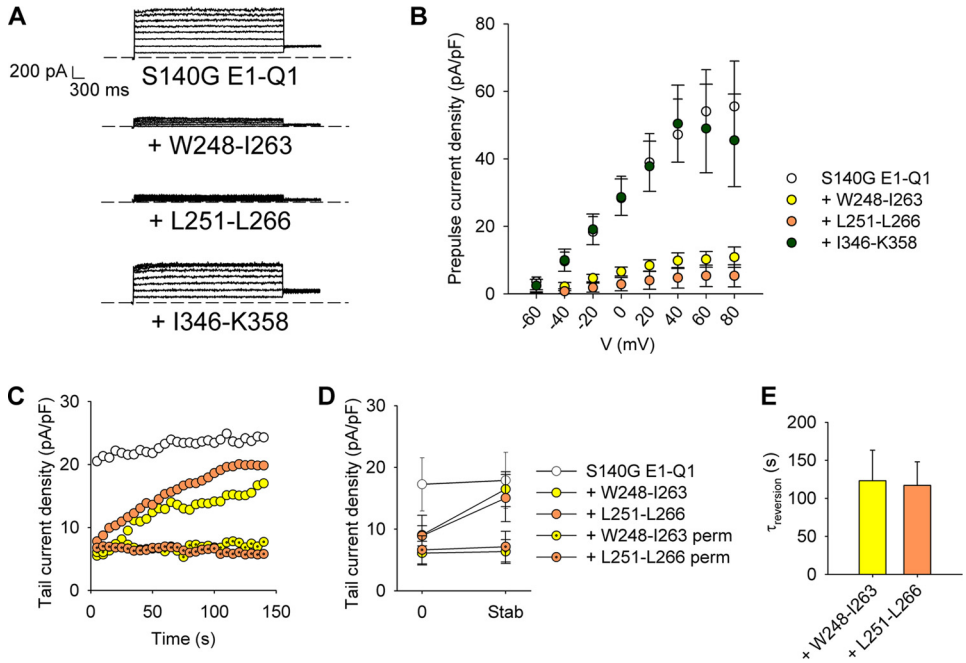

FIGURE 6. **Effects of the $S4S5_L$ or the $S6_T$ peptides on S140G E1-Q1 currents.** *A*, representative ruptured patch recordings of the S140G E1-Q1 current in the absence (S140G E1-Q1) and in the presence of $S4S5_L$ peptides (+ Trp^{248}–Ile^{263} or + Leu^{251}–Leu^{266}) or a $S6_T$ peptide (+ Ile^{346}–Lys^{358}). The voltage protocol was the same as described in the legend to Fig. 2. *B*, S140G E1-Q1 current density measured on the late current ($n = 9–21$). *C*, S140G E1-Q1 tail current density measured at −40 mV after a prepulse at +40 mV during dilution of $S4S5_L$ peptides and in permeabilized configuration (*perm*) ($n = 8$) in representative cells. Voltage protocol was from a holding potential of −80 mV, one voltage step to +40 mV (1000 ms) and then back to −40 mV (500 ms), every 5 s. *D*, mean tail-current density measured as in *C*, immediately after patch rupture/permeabilization (0) and after current stabilization (*stab*). *E*, reversion time constant ($\tau_{reversion}$) determined from a monoexponential fit of the run-up in the conditions presented in *C* ($n = 6–8$).

peptides, patch rupture led to a gradual increase in current density (Fig. 6, *C–E*), consistent with the peptide dilution into the patch pipette, as observed for the WT channel above. Current recovery did not occur when peptide dilution was prevented using the permeabilized patch configuration (Fig. 6, *C* and *D*). It is worth noting that the current increased toward values similar to those observed in the absence of peptide indicating that the peptides affect channel gating but not trafficking. Importantly, the reversion of the peptide effects indicates a loose peptide/channel association consistent with a loose $S4S5_L/S6_T$ interaction in the channel.

$S4S5_L$ and $S6_T$ Peptides Interact with Each Other—Our observations suggest an interaction between $S4S5_L$ and $S6_T$ in the channel protein. Accordingly, when the two peptides are coexpressed, they should bind to each other and annihilate their respective effect. To confirm this, we used the S140G E1-Q1 mutant, which is sensitive to the $S4S5_L$ but not the $S6_T$ peptides. When both a $S4S5_L$ (Trp^{248}–Ile^{263} or Leu^{251}–Leu^{266}) and a $S6_T$ peptide (Ile^{346}–Lys^{358}) were coexpressed with the channel, the inhibition of S140G E1-Q1 by a $S4S5_L$ peptide was not observed (Fig. 7). This loss of inhibition is consistent with the idea that the $S6_T$ peptide Ile^{346}–Lys^{358} associates with the $S4S5_L$ peptide and competitively prevents $S4S5_L$ peptide association with the channel $S6_T$. Hence, $S4S5_L$ and $S6_T$ peptides that bind the WT channel can also bind to each other. Interestingly, the effects of $S4S5_L$ peptides are not prevented by the $S6_T$ peptide Phe^{340}–Ala^{352} that does not up-regulate the WT KCNE1-KCNQ1 channel either. This suggests that the $S6_T$ peptide that does not bind the WT

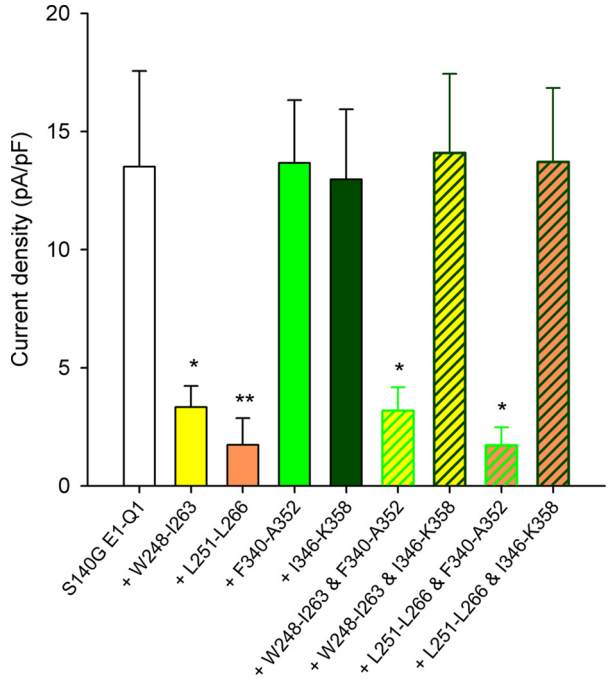

FIGURE 7. **Interaction between $S4S5_L$ and $S6_T$ peptides probed by S140G.** S140G E1-Q1 tail current densities in the absence (S140G E1-Q1) and in the presence of various $S4S5_L$ or/and $S6_T$ peptides suggesting interactions between Leu^{251}–Leu^{266} and Ile^{346}–Lys^{358}, Trp^{248}–Ile^{263} and Ile^{346}–Lys^{358} and the lack of interaction between Leu^{251}–Leu^{266} and Phe^{340}–Ala^{352}, and between Trp^{248}–Ile^{263} and Phe^{340}–Ala^{352} ($n = 9–13$). *, $p < 0.05$; **, $p < 0.01$ *versus* S140G E1-Q1.

KCNE1-KCNQ1 channel cannot bind the $S4S5_L$ peptide either, further confirming the specificity of the $S4S5_L/S6_T$ interaction.

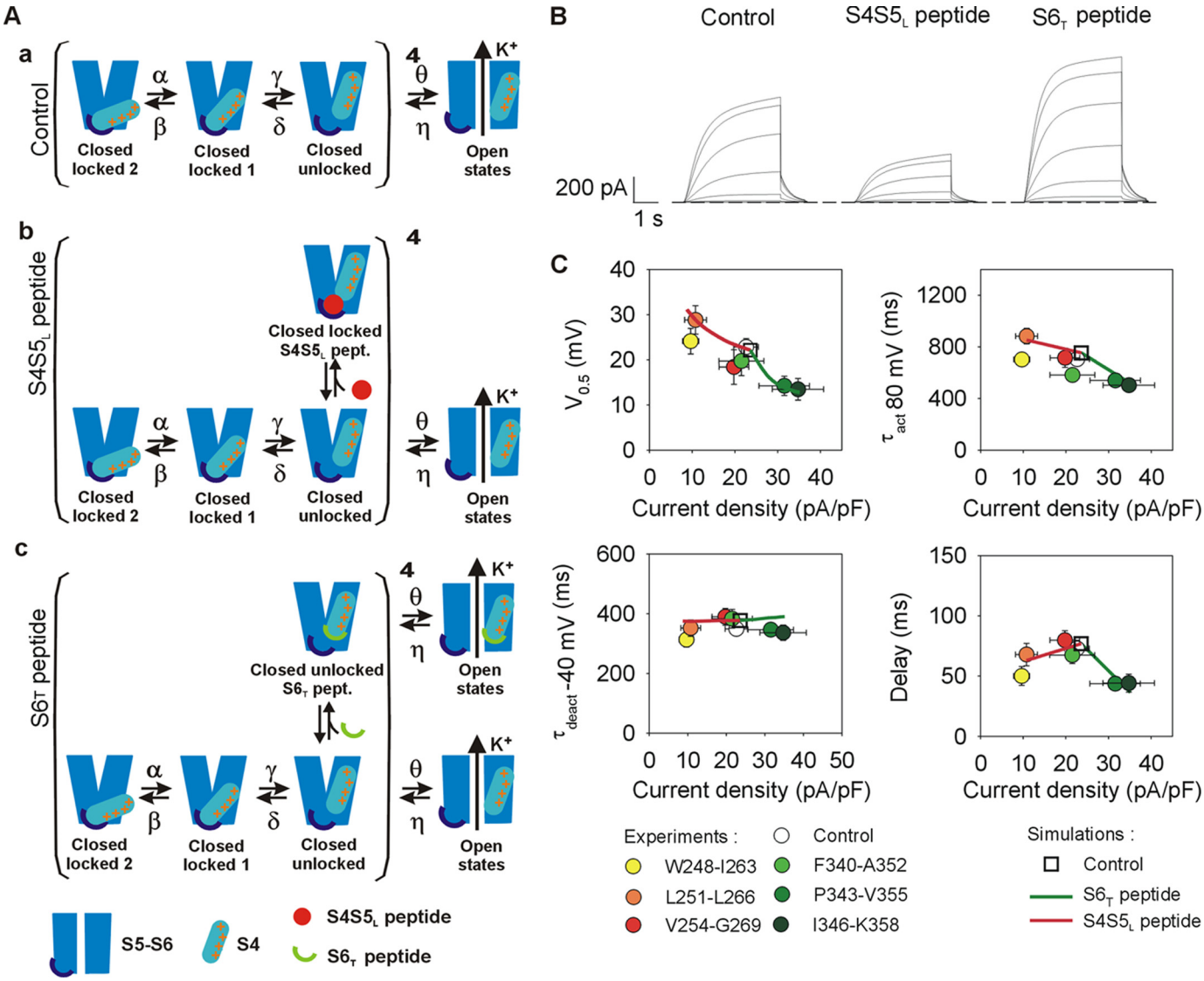

FIGURE 8. **Kinetic model of KCNE1-KCNQ1 and its interactions with $S4S5_L$ or $S6_T$ peptide.** *A*, kinetic model scheme. This model is based on Rudy's model for the KCNE1-KCNQ1 tetramer (18). We hypothesize that the unbinding of the $S4S5_L$ and $S6_T$ domains unlocks the channel and corresponds to the last transition of the closed channel (closed locked 1 state to closed unlocked state). Peptides are likely to interact with each monomer in the unlocked states. The model covers three experimental conditions: absence of peptide (*panel a*), presence of $S4S5_L$ peptides (*panel b*) and presence of $S6_T$ peptides (*panel c*). Optimized transition rates are presented in Table 1. *B*, simulated currents during step protocols in the absence (*Control*) or the presence of $S4S5_L$ or $S6_T$ peptide. *C*, comparison between simulated and experimental half-activation potentials, activation kinetics, deactivation kinetics, and delay of activation *versus* current density. The changes of these parameters driven by the peptides are well described by the model. The continuum of simulated results in presence of peptides (*solid lines*) is obtained by varying the binding rates of the peptides.

$S4S5_L$/$S6_T$ Interaction Is Channel-specific—To establish the channel specificity of the $S4S5_L$ peptide Leu^{251}–Leu^{266} and the $S6_T$ peptide Ile^{346}–Lys^{358} for KCNE1-KCNQ1, we tested their potential effects on hERG, another voltage-gated potassium channel. As shown in the supplemental Fig. 1, KCNQ1 $S4S5_L$ and $S6_T$ peptides had no effect on hERG current amplitude and half-activation potential, confirming that peptides are channel-specific.

A Kinetic Model Describes Observed Data for All Peptides—To test the consistency between the hypothesis and the altered biophysical parameters in the presence of the peptide, we developed a kinetic model to describe the peptide-induced alterations in KCNE1-KCNQ1 channel properties (18). We deliberately made the peptides bind only the closed state immediately preceding the concerted opening (Fig. 8, *A*, *panels b* and *c*) because, in the other closed states, the proximity of the endogenous $S4S5_L$ and $S6_T$ is supposed to prevent peptides access. In the model, the $S4S5_L$ peptide mimics the endogenous $S4S5_L$ linker and locks the channel in a closed state. Conversely, the $S6_T$ peptide decoys the endogenous $S4S5_L$ peptide and limits this locking. This theoretical model fits the observed data; the peptides affect not only the current amplitude but also the half activation potential and the activation kinetics, and they do not affect the deactivation kinetics (Fig. 8, *B* and *C*). The kinetic model also illustrates that peptides binding prevents the channel from going to deep closed state (especially closed locked 2 in Fig. 8*A*). This should provoke a reduction in the delay of channel activation (17). Indeed, the delay measured in the current recordings was similar to the delay calculated in the

model, further validating the model and the specificity of the peptides effects (Fig. 8*C*).

DISCUSSION

Altogether, our results show that $S4S5_L$ acts as an inhibiting ligand that binds with low affinity to $S6_T$ only at negative potentials, locking the S5-S6 pore domain in a closed state. The state-dependent interaction between $S4S5_L$ and $S6_T$ has already been proposed by Ferrer *et al.* (9) for hERG, another delayed rectifier potassium channel. This idea was suggested by the fact that a covalent link between $S4S5_L$ and $S6_T$ stabilizes the hERG closed state (9). If $S4S5_L$ and $S6_T$ interact in both the closed and open states, a covalent interaction should not lead to channel closure. If, conversely, $S4S5_L$ interacts with S6 only in the closed state, one expects that forcing $S4S5_L$ interaction with S6 closes the channel.

In the present study, we propose a similar state-dependent interaction between $S4S5_L$ and $S6_T$ in KCNQ1 channels and provide a mechanistic scheme in which a ligand attached to S4 ($S4S5_L$) interacts with the pore and locks it closed in a voltage-dependent fashion. This mechanism supports the functional model in which the six-transmembrane domain KCNQ1 channels may be regarded as the fusion of a voltage sensor domain (S1-S4) and a ligand-gated channel (S5-S6) very similar to a two-transmembrane domain channel.

In this model, the vicinity between $S4S5_L$ and $S6_T$ in the closed state suggests that the interaction between $S4S5_L$ and $S6_T$ is loose enough to allow $S4S5_L/S6_T$ unbinding upon depolarization. We tried to confirm this by biochemical methods using synthetic MG Leu^{251}–Leu^{266} and MG Ile^{346}–Lys^{358} peptides, but we could not solubilize the peptides at concentrations >100 μM and did not observe any interaction using differential ultracentrifugation and native gels. One possibility is that the cytosol provides an environment to solubilize the peptide in the millimolar range and that this range must be reached to uncover the peptide-peptide or peptide-channel interaction. Importantly, proteins expressed under the control of a CMV promoter can reach expression levels in the millimolar range (27, 28). Yeast two hybrid technique was also used to probe the $S4S5_L$ and $S6_T$ peptides interaction in a "cytosolic" environment but no interaction between Leu^{251}–Leu^{266} and Ile^{346}–Lys^{358} could be detected. The later result is probably because of the weakness of the interaction and the poor sensitivity of the technique. Nevertheless, although chemical and biochemical approaches failed to demonstrate direct $S4S5_L/S6_T$ interaction, our experiments analyzing the effects of Val^{254} and Leu^{353} point mutations (Figs. 4 and 5), the $S4S5_L/S6_T$ peptide interaction (Fig. 7), and channel specificity (supplemental Fig. 1) strongly support this interaction. Importantly, all of these results are consistent with a loose interaction between $S4S5_L$ and $S6_T$.

Interestingly, the ligand/receptor mechanism we propose in this study may explain the surprising observation that hyperpolarization-activated channels have a similar voltage sensor domain as depolarization-activated channels but an opposite response to depolarization. In the hyperpolarization-activated channel KAT1 (7) and HCN (29), $S4S5_L$ has also been suggested to couple voltage sensing and pore opening by a labile binding (29). Similar to our model where $S4S5_L$ binds $S6_T$ in the closed state, the $S4S5_L/S6$ interaction seems present only in the open state of KAT1 and HCN (7, 8). This would explain why the latter channels are closed by membrane depolarization. The state-dependent interaction between $S4S5_L$ and $S6_T$ observed in hERG, KAT1, HCN, and now in KCNQ1 channels suggest that the mechanism described here may be applied to other voltage-gated potassium channels and probably sodium and calcium channels, which share the same overall structure with Kv tetramers.

In summary, the activation mechanism suggested here describes the pore domain as being locked closed at rest by the binding of a ligand ($S4S5_L$) to the gate ($S6_T$). Upon plasma membrane depolarization, S4 pulls $S4S5_L$ away from $S6_T$, allowing channel opening. Other molecular mechanisms will have to be taken into account to fully understand the complex voltage dependence, like the molecular events accompanying the concerted channel opening triggered by S4 movement (30).

Generally, application of the ligand/receptor mechanism to voltage-gated ion channels may lead to the design of peptides specifically down- or up-regulating one specific type of ion channel. This may open new therapeutic avenues to treat channelopathies.

Acknowledgments—We thank Béatrice Leray, Marie-Joseph Louérat, and Agnès Carcouët for expert technical assistance.

REFERENCES

1. Jiang, Y., Ruta, V., Chen, J., Lee, A., and MacKinnon, R. (2003) *Nature* **423,** 42–48
2. Jiang, Y., Lee, A., Chen, J., Ruta, V., Cadene, M., Chait, B. T., and MacKinnon, R. (2003) *Nature* **423,** 33–41
3. Long, S. B., Campbell, E. B., and Mackinnon, R. (2005) *Science* **309,** 903–908
4. Ahern, C. A., and Horn, R. (2004) *Trends Neurosci.* **27,** 303–307
5. Doyle, D. A., Morais Cabral, J., Pfuetzner, R. A., Kuo, A., Gulbis, J. M., Cohen, S. L., Chait, B. T., and MacKinnon, R. (1998) *Science* **280,** 69–77
6. Kuo, A., Gulbis, J. M., Antcliff, J. F., Rahman, T., Lowe, E. D., Zimmer, J., Cuthbertson, J., Ashcroft, F. M., Ezaki, T., and Doyle, D. A. (2003) *Science* **300,** 1922–1926
7. Grabe, M., Lai, H. C., Jain, M., Jan, Y. N., and Jan, L. Y. (2007) *Nature* **445,** 550–553
8. Prole, D. L., and Yellen, G. (2006) *J. Gen. Physiol.* **128,** 273–282
9. Ferrer, T., Rupp, J., Piper, D. R., and Tristani-Firouzi, M. (2006) *J. Biol. Chem.* **281,** 12858–12864
10. Barhanin, J., Lesage, F., Guillemare, E., Fink, M., Lazdunski, M., and Romey, G. (1996) *Nature* **384,** 78–80
11. Sanguinetti, M. C., Curran, M. E., Zou, A., Shen, J., Spector, P. S., Atkinson, D. L., and Keating, M. T. (1996) *Nature* **384,** 80–83
12. Boulet, I. R., Labro, A. J., Raes, A. L., and Snyders, D. J. (2007) *J. Physiol.* **585,** 325–337
13. John, S. A., Weiss, J. N., Xie, L. H., and Ribalet, B. (2003) *J. Physiol.* **552,** 23–34
14. Gilchrist, A., Li, A., and Hamm, H. E. (2002) *Sci. STKE.* **2002,** PL1
15. Le Maout, S., Welling, P. A., Brejon, M., Olsen, O., and Merot, J. (2001) *Proc. Natl. Acad. Sci. U.S.A.* **98,** 10475–10480
16. Bellocq, C., Wilders, R., Schott, J. J., Louérat-Oriou, B., Boisseau, P., Le Marec, H., Escande, D., and Baró, I. (2004) *Mol. Pharmacol.* **66,** 1093–1102
17. Cole, K. S., and Moore, J. W. (1960) *Biophys. J.* **1,** 1–14
18. Silva, J., and Rudy, Y. (2005) *Circulation* **112,** 1384–1391

19. Lu, Z., Klem, A. M., and Ramu, Y. (2001) *Nature* **413,** 809–813
20. Lu, Z., Klem, A. M., and Ramu, Y. (2002) *J. Gen. Physiol.* **120,** 663–676
21. Wang, W., Xia, J., and Kass, R. S. (1998) *J. Biol. Chem.* **273,** 34069–34074
22. Park, K. H., Piron, J., Dahimene, S., Mérot, J., Baró, I., Escande, D., and Loussouarn, G. (2005) *Circ. Res.* **96,** 730–739
23. Loussouarn, G., Baró, I., and Escande, D. (2006) *Methods Mol. Biol.* **337,** 167–183
24. Kang, C., Tian, C., Sönnichsen, F. D., Smith, J. A., Meiler, J., George, A. L., Jr., Vanoye, C. G., Kim, H. J., and Sanders, C. R. (2008) *Biochemistry* **47,** 7999–8006
25. Zheng, R., Thompson, K., Obeng-Gyimah, E., Alessi, D. M., Chen, J., Cheng, H., and McDonald, T. V. (2010) *Biochem. J.* **428,** 75–84
26. Chen, Y. H., Xu, S. J., Bendahhou, S., Wang, X. L., Wang, Y., Xu, W. Y., Jin, H. W., Sun, H., Su, X. Y., Zhuang, Q. N., Yang, Y. Q., Li, Y. B., Liu, Y., Xu, H. J., Li, X. F., Ma, N., Mou, C. P., Chen, Z., Barhanin, J., and Huang, W. (2003) *Science* **299,** 251–254
27. Lin, P., Luby-Phelps, K., and Stull, J. T. (1999) *J. Biol. Chem.* **274,** 5987–5994
28. Rex, T. S., Peet, J. A., Surace, E. M., Calvert, P. D., Nikonov, S. S., Lyubarsky, A. L., Bendo, E., Hughes, T., Pugh, E. N., Jr., and Bennett, J. (2005) *Mol. Vis.* **11,** 1236–1245
29. Chen, J., Mitcheson, J. S., Tristani-Firouzi, M., Lin, M., and Sanguinetti, M. C. (2001) *Proc. Natl. Acad. Sci. U.S.A.* **98,** 11277–11282
30. Soler-Llavina, G. J., Chang, T. H., and Swartz, K. J. (2006) *Neuron* **52,** 623–634
31. Labro, A. J., Boulet, I. R., Choveau, F., Mayeur, E., Bruyns, T., Loussouarn, G., Raes, A. L., and Snyders, D. J. (2010) *J. Biol. Chem.* **285,** 717–726